What Makes a Boundary Less Accessible

D. S. Grebenkov*

Unité de Recherche en Résonance Magnétique Médicale, CNRS-Université Paris-Sud, 91405 Orsay, France

(Received 27 July 2005; published 10 November 2005)

For the growth and transport processes driven by Laplacian fields, the accessibility of an interface for Brownian motion is characterized by the harmonic measure. Its multifractal properties help one to understand how the irregular geometry of biological membranes, metallic electrodes, porous catalysts, or growing aggregates is ''seen'' by diffusing particles. To clarify this point, we performed an extensive numerical study of the harmonic measure on two families of self-similar triangular Koch curves of variable Hausdorff dimension which may represent branched pore networks or fjordlike rough interfaces. Although these structures are apparently different, the multifractal properties of the harmonic measure in two cases are found to be very close for curves of small Hausdorff dimensions and to differ for higher irregularity. This provides new insight into optimization problems in chemical engineering.

DOI: 10.1103/PhysRevLett.95.200602 PACS numbers: 05.60.−k, 02.50.−r, 05.10.−a

Various transport phenomena in nature and chemical industry are governed by Laplacian fields. Examples can be found in physiology (oxygen diffusion towards and across alveolar tissue in pulmonary acinus), in electrochemistry (electric current through metallic electrodes into electrolyte), and in petrochemistry (diffusion of reactive molecules towards catalytic surface) [1]. To increase the overall diffusive flux, the interface geometry is often made, naturally or artificially, very irregular. This is the case of porous catalysts, rough metallic electrodes, or tortuous mammal acini. However, the transfer or reactive capacity of an interface is crucially limited by its accessibility for the Brownian motion. This effect known as *diffusional screening* may have positive or negative consequences for practical applications. For example, it bounds the overall production of species in the diffusion-limited regime of heterogeneous catalysis but allows one to design long-working catalysts [2]. The adaptive regularization of the lung respiratory efficiency is also related to this effect [3–6].

The accessibility of a boundary for diffusing particles is mathematically characterized by the harmonic measure also known as primary current distribution in electrochemistry. For any (Borel) subset of the boundary, its harmonic measure is defined as the probability for the Brownian motion started from a distant source to hit the boundary for the first time on this subset [7–9]. For a smooth boundary, the distribution of the harmonic measure is completely determined by its density (in electrostatics, this function gives the electric charge distribution on a metallic surface induced by a distant charge). The presence of a *simple* geometrical irregularity is reflected in a singular behavior of this density. For instance, the probability to hit a wedge of angle θ within a vicinity of diameter δ decreases as δ^{α} for vanishing δ, where

$$\alpha = \pi/\theta. \tag{1}$$

The exponent α permits one to characterize the ''accessibility strength'' or ''screening capacity'' of this irregularity in the sense that sharp angles (higher α) are less accessible (more screened) for diffusing particles than obtuse ones (lower α). In this light, the most accessible angle is a needle with $\theta = 2\pi$, so that $\alpha_{\min} = 1/2$ in agreement with Beurling's theorem [10].

For a rough interface, almost each boundary point leads to a singularity, so that the harmonic measure *density* does not exist (while the measure itself is well defined). Being locally still characterized by their ''strengths,'' the boundary points of the same α can be grouped into a subset S_α. The Hausdorff dimensions $f(\alpha)$ of different subsets S_α of the boundary form the *multifractal spectrum* of the harmonic measure. Roughly speaking, while α quantifies the accessibility ''strength'' of boundary points in S_α, the function $f(\alpha)$ shows how ''big'' this subset is. In particular, the maximum value of $f(\alpha)$ gives the Hausdorff dimension D_0 of the boundary, a measure of its geometrical complexity.

Although the multifractal properties of the harmonic measure were studied enough, the relation between the geometry itself and its multifractal spectrum is still obscure. Is a more irregular boundary (greater D_0) more screened? How does the presence of deep fjords or a pore network modify the surface accessibility? More generally, what makes a boundary less accessible? The last question, which originated the present Letter, is closely related to different optimization problems in chemical engineering.

Without pretending to give complete answers to these fundamental questions, we are going to clarify certain points. For this purpose, the harmonic measure ω has been studied numerically on two families of self-similar triangular Koch curves obtained iteratively from the same generator shown in Fig. 1. The Hausdorff dimension $D_0^{(\phi)}$ of these curves can be varied continuously from 1 to 2 by changing the angle ϕ between two intermediate segments from π to 0:

$$D_0^{(\phi)} = \frac{\ln 4}{\ln(2 + 2\sin\phi/2)}. \quad (2)$$

Depending on the side which is exposed to diffusing particles, the shape of these curves is very different so that one can speak about the two families. Starting from a distant source at the top of Fig. 1, the particles *progressively* penetrate into smaller and smaller pores of the material. Such curves could mimic the geometry of a branched pore network and are called "top seen." In contrast, the diffusing particles started at the bottom of Fig. 1 arrive onto a rough surface with a fjordlike pore structure. The curves of this family are called "bottom seen."

The numerical simulations have been realized for the first ten generations of these curves with different angles ϕ. For fixed generation order g and angle ϕ, the curve is covered by a finite number of compact disjoint sets Γ_k^δ of a chosen diameter δ. The trajectories of the Brownian motion were modeled with the help of the geometry-adapted fast random walk algorithm developed originally for the quadratic Koch curve and described in detail in [11]. Starting from a distant source, a diffusing particle executes a series of random jumps in the bulk. The jump length at each step is equal to the distance between the current position and the boundary. This distance is calculated explicitly for the first generation, while the self-similarity of the Koch curves allows one to estimate it for higher generations. Periodic boundary conditions are imposed on the left and right vertical borders. The particle is considered as absorbed on a small region $S \cap \Gamma_k^\delta$ of the boundary, when the distance to this region from the current position

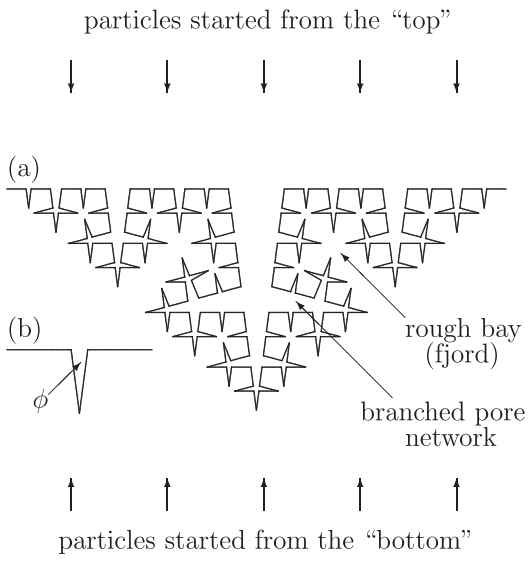

FIG. 1. (a) Fourth generation of the self-similar triangular Koch curve with the Hausdorff dimension $D_0 \simeq 1.7$. Depending on the side exposed to diffusing particles, this curve allows one to model either branched pore networks (source at the "top") or fjordlike rough bays (source at the "bottom"). (b) Generator of this curve is composed of four identical linear segments with the angle $\phi = \pi/12$ between intermediate segments.

becomes smaller than a chosen threshold value. Repeating the above trajectory simulation N times, one approximates the hitting probabilities $p_{k,\delta} = \omega\{S \cap \Gamma_k^\delta\}$ by frequencies of absorptions on different regions. We used $N = 10^{10}$, which allows one to calculate the positive order moments

$$\zeta^{(\phi)}(q, \delta) = \sum_k (p_{k,\delta})^q \quad (3)$$

with five significant digits. The scale δ is ranged between the diameter of the curve $L = 1$ and the smallest segment length γ^{-g} for the chosen generation order g, where $\gamma = 2[1 + \sin(\phi/2)]$ is the homothety ratio. The use of the logarithmic development [11] ensures an accurate computation of the multifractal exponents $\tau^{(\phi)}(q)$ of the harmonic measure:

$$\tau^{(\phi)}(q) = \lim_{\delta \to 0} \frac{\ln \zeta^{(\phi)}(q, \delta)}{\ln \delta}. \quad (4)$$

These exponents are related to the multifractal spectrum $f^{(\phi)}(\alpha)$ by Legendre transform [12]:

$$f^{(\phi)}(\alpha) = \min_q \{q\alpha - \tau^{(\phi)}(q)\}. \quad (5)$$

For convenience, the multifractal dimensions are often introduced as $D_q^{(\phi)} = \tau^{(\phi)}(q)/(q - 1)$.

As a numerical test for the accuracy of the above numerical technique, we first calculated the information dimension $D_1^{(\phi)}$ for both families of Koch curves with the Hausdorff dimension $D_0^{(\phi)}$ ranging between 1.01 and 1.99. The Makarov theorem states that $D_1 = 1$ for any simply connected set in the plane; i.e., the Hausdorff dimension of the support of the harmonic measure is equal to 1 [13,14]. In full agreement with this mathematical result, the computed values $D_1^{(\phi)}$ for all studied curves equal unity with a deviation smaller than 10^{-3}. Since the statement $D_1 = 1$ presents a truly nontrivial condition for the calculated distributions, this test confirms the validity of the following numerical results.

The dependence of the other multifractal dimensions $D_q^{(\phi)}$ on the Hausdorff dimension $D_0^{(\phi)}$ is shown in Fig. 2. The first and quite surprising result is that the multifractal dimensions $D_q^{(\phi)}$ turn out to be identical for the top-seen and bottom-seen curves of the same Hausdorff dimension when $D_0^{(\phi)} \lesssim 1.3$. Being quite different geometrically, these two types of morphologies are essentially indistinguishable for diffusing particles, i.e., when they are "seen" by the harmonic measure. At the same time, the spatial distributions of hitting probabilities $\{p_{k,\delta}\}$ over these two boundaries are very different. However, from a certain value of $D_0^{(\phi)}$, the multifractal dimensions for the top-seen and bottom-seen curves are separated. In the former case, these dimensions approach 1, while in the latter one, they converge to smaller values. Their different limits can be explained by a simple geometrical argument. When the angle ϕ goes to 0, the channels of the top-seen curves

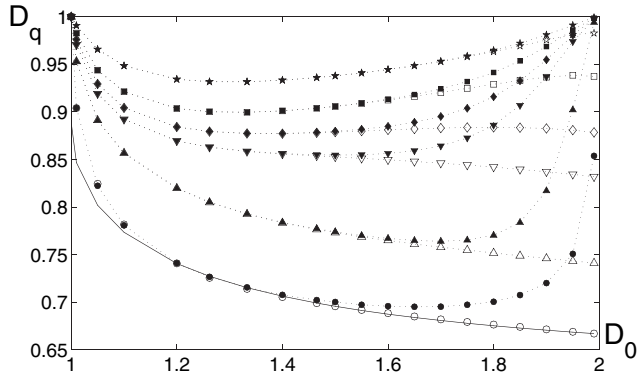

FIG. 2. Positive order multifractal dimensions of the harmonic measure on the top-seen (solid symbols) and bottom-seen (open symbols) triangular Koch curves: $q = 2$ (stars), $q = 3$ (squares), $q = 4$ (diamonds), $q = 5$ (up-pointing triangles), $q = 10$ (down-pointing triangles), and $q = \infty$ (circles). For comparison, the dependence (6) of $D_\infty^{(\phi)}$ for the bottom-seen curves is drawn by a solid line. Dotted lines are a guide to the eye.

become progressively thinner, and the harmonic measure is concentrated on horizontal segments almost uniformly. Such a distribution is not essentially different from that on a simple linear segment. As a result, all multifractal dimensions seem to converge to 1. In contrast, the bottom-seen curves approach staircase shapes as $\phi \to 0$, so that the multifractal dimensions $D_q^{(\phi)}$ converge to nontrivial values $D_q^{(\phi=0)}$.

When the moment order q increases, the contribution of small hitting probabilities progressively vanishes. In the limit $q \to \infty$, the only maximum probability $p_{\max}$ contributes, so that the multifractal dimension $D_\infty^{(\phi)}$ describes its scaling behavior: $p_{\max} \propto \delta^{D_\infty^{(\phi)}}$ as $\delta \to 0$. This is the lowest bound of $D_q^{(\phi)}$ and, consequently, the smallest value of the strength for the Koch boundaries: $\alpha_{\min}^{(\phi)} = D_\infty^{(\phi)}$. For the bottom-seen curves, the maximum hitting probability corresponds to the upper corner (with obtuse angle $2\pi - \phi$), so that one may expect to find the scaling exponent $D_\infty^{(\phi)}$ to be $\pi/(2\pi - \phi)$, as in the case of a simple wedge singularity. However, the self-similar structure of the Koch curve leads to a different result. Indeed, the presence of a number of other angles in a close vicinity of this corner makes the scaling of the harmonic measure less sharp. For the bottom-seen curves, the following simple relation provides a very good fit for the numerical data (see Fig. 2):

$$D_\infty^{(\phi)} \simeq \frac{2}{3}\,\frac{1}{1 - \phi/4\pi}. \tag{6}$$

This scaling behavior formally corresponds to a wedge singularity with the obtuse angle $\theta = 3\pi/2 - 3\phi/8$. In particular, in the limit of the staircase shapes ($\phi \to 0$ and $D_0^{(\phi)} \to 2$), the maximum hitting probability corresponding to the right angle has the scaling exponent $D_\infty^{(\phi=0)} = 2/3$, in perfect agreement with our numerical results.

For large enough q, the contribution of the maximum hitting probability is still dominant, and one may use the simplest approximation $\zeta^{(\phi)}(q, \delta) \propto (p_{\max})^q \propto \delta^{qD_\infty^{(\phi)}}$ to obtain

$$D_q^{(\phi)} \simeq D_\infty^{(\phi)} + \frac{D_\infty^{(\phi)}}{q - 1}. \tag{7}$$

Although this asymptotic relation gives a false value for the correlation dimension ($q = 2$), it becomes accurate for the multifractal dimensions of higher orders as shown in Fig. 3. The simple form of the asymptotic behavior (7) may be related to the *deterministic* self-similarity of the triangular Koch curves. In contrast, the stochastic boundaries such as percolation clusters [15,16] or diffusion-limited aggregates [17–19] exhibit different asymptotic behaviors.

The negative orders q accentuate the contribution of small hitting probabilities. In the limit $q \to -\infty$, the only minimum probability $p_{\min}$ contributes to $\zeta^{(\phi)}(q, \delta)$, $D_{-\infty}^{(\phi)}$ characterizes its scaling behavior, $p_{\min} \propto \delta^{D_{-\infty}^{(\phi)}}$ (as $\delta \to 0$), and one has $\alpha_{\max}^{(\phi)} = D_{-\infty}^{(\phi)}$. However, an accurate computation of $p_{\min}$ presents a difficult problem since this probability decreases very rapidly with the generation order g and Hausdorff dimension $D_0^{(\phi)}$. The same difficulty concerns the computation of the negative order moments. For this reason, we had to limit ourselves to the curves with $D_0^{(\phi)} \le 4/3$. Even for the case $D_0^{(\phi)} = 4/3$, the negative order multifractal dimensions for the top-seen and bottom-seen curves are close to each other (Fig. 3), and they are almost indistinguishable for smaller Hausdorff dimensions. In contrast, a more pronounced difference would be expected for larger $D_0^{(\phi)}$. As shown in Fig. 3, the asymptotic behavior (7) can also be applied in the limit $q \to -\infty$, if $D_\infty^{(\phi)}$ is replaced by $D_{-\infty}^{(\phi)}$. For the top-seen triangular Koch curves, the minimum hitting probability is located at the deepest vertex of the angle ϕ, so that one may expect $D_{-\infty}^{(\phi)} \simeq \pi/\phi$. The numerical simulations sug-

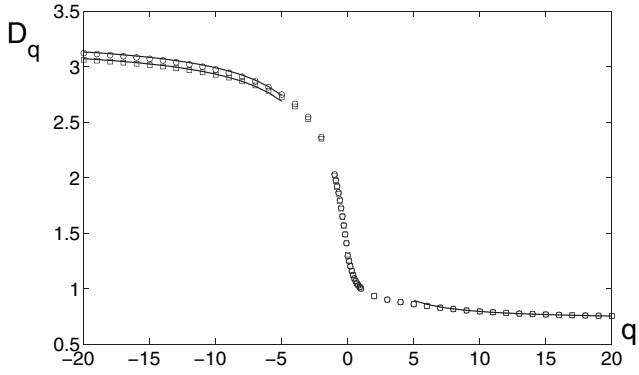

FIG. 3. Multifractal dimensions $D_q^{(\phi)}$ of the harmonic measure as functions of the order q for bottom-seen (squares) and top-seen (circles) curves with $D_0^{(\phi)} = 4/3$. The solid lines represent the asymptotic behavior (7).

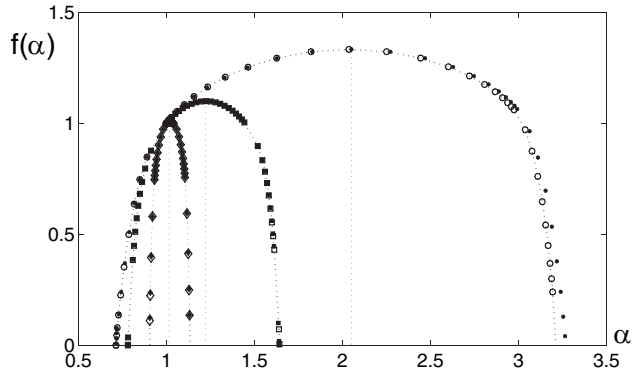

FIG. 4. Multifractal spectra for top-seen (open symbols) and bottom-seen (solid symbols) curves of different Hausdorff dimensions: $D_0^{(\phi)} = 1.01$ (diamonds), $D^{(\phi)} = 1.10$ (squares), and $D_0^{(\phi)} = 4/3$ (circles). The vertical dotted lines indicate the reflection symmetry of these spectra.

gest $D_{-\infty}^{(\phi)} \simeq \pi/\theta$ with $\theta \simeq \phi/0.9$. It means that the harmonic measure "sees" a larger angle than ϕ due to the presence of other corners in close vicinity.

Finally, the multifractal spectra $f(\alpha)$ for the top-seen and bottom-seen curves of different Hausdorff dimensions are presented in Fig. 4. Since the computation of the right-hand side of these spectra involves the negative order moments, the only moderate Hausdorff dimensions were considered. The first observation is that the multifractal spectra for both curves of the same Hausdorff dimension are identical for $D_0^{(\phi)} = 1.01$ and $D_0^{(\phi)} = 1.10$, while their right-hand sides become slightly different for $D_0^{(\phi)} = 4/3$. For larger $D_0^{(\phi)}$, a higher difference between these spectra is expected due to the above analysis of multifractal dimensions. Interestingly, the multifractal spectra seem to be symmetric with respect to reflection at a vertical line, i.e., $f(\alpha) \simeq f(2\alpha_0 - \alpha)$, where α_0 depends on $D_0^{(\phi)}$, providing the maximum of the spectrum: $f(\alpha_0) = D_0^{(\phi)}$. Since the multifractal dimensions for the top-seen and bottom-seen curves become different for larger $D_0^{(\phi)}$, this symmetry would be broken, at least for one of these two families. This question remains open for the moment.

In conclusion, we draw attention to the two following results. First, the Hausdorff dimension $D_0^{(\phi)}$, as a measure of the geometrical complexity, is not determinant for the diffusional screening: the harmonic measure on the top-seen curves with $D_0^{(\phi)}$ close to 2 exhibits almost the same scaling behavior as on a smooth boundary since $D_q^{(\phi)}$ converge to 1. This result provides new insight into practical applications, e.g., in chemical engineering. Indeed, it shows that one does not need to explore very irregular shapes to diminish the multifractal dimensions. Second, the multifractal dimensions and multifractal spectrum of the harmonic measure on the top-seen and bottom-seen curves are identical for moderate values of $D_0^{(\phi)}$. This means that the harmonic measure is not sensitive enough to distinguish these boundaries of quite different geometry. The hierarchical self-similar structure of these curves is thus more determinant than their geometrical details.

*Electronic address: denis.grebenkov@polytechnique.edu

[1] B. Sapoval, in *Fractals and Disordered Systems*, edited by A. Bunde and S. Havlin (Springer, New York, 1996), pp. 233–261.
[2] M.-O. Coppens, Catalysis Today **53**, 225 (1999).
[3] B. Sapoval, E. R. Weibel, and M. Filoche, in *Fractals in Biology and Medicine*, edited by G. A. Losa, D. Merlini, T. F. Nonennmacher, and E. R. Weibel (Birkhauser, Bâle, 2002), pp. 25–38.
[4] M. Felici, M. Filoche, and B. Sapoval, J. Appl. Physiol. **94**, 2010 (2003).
[5] D. S. Grebenkov, M. Filoche, B. Sapoval, and M. Felici, Phys. Rev. Lett. **94**, 050602 (2005).
[6] M. Felici, M. Filoche, C. Straus, T. Similowski, and B. Sapoval, Respir. Physiolo. Neurobio. **145**, 279 (2005).
[7] J. B. Garnett, *Applications of Harmonic Measure* (John Wiley & Sons, New York, 1986).
[8] N. G. Makarov, St. Petersburg Math. J. **10**, 217 (1999).
[9] J. B. Garnett and D. E. Marshall, *Harmonic Measure* (Cambridge University Press, Cambridge, 2005).
[10] L. V. Ahlfors, *Conformal Invariants: Topics in Geometric Function Theory* (McGraw-Hill, New York, 1973).
[11] D. S. Grebenkov, A. A. Lebedev, M. Filoche, and B. Sapoval, Phys. Rev. E **71**, 056121 (2005).
[12] T. C. Halsey, M. H. Jensen, L. P. Kadanoff, I. Procaccia, and B. I. Shraiman, Phys. Rev. A **33**, 1141 (1986).
[13] N. G. Makarov, Proc. London Math. Soc. **51**, 369 (1985).
[14] P. Jones and T. Wolff, Acta Math. **161**, 131 (1988).
[15] B. Duplantier, Phys. Rev. Lett. **82**, 3940 (1999); **82**, 880 (1999); **84**, 1363 (2000).
[16] B. Duplantier, J. Stat. Phys. **110**, 691 (2003).
[17] B. B. Mandelbrot and C. J. G. Evertsz, Nature (London) **348**, 143 (1990).
[18] M. H. Jensen, A. Levermann, J. Mathiesen, and I. Procaccia, Phys. Rev. E **65**, 046109 (2002).
[19] M. H. Jensen, J. Mathiesen, and I. Procaccia, Phys. Rev. E **67**, 042402 (2003).